Iranian Journal of Electrical and Electronic Engineering 01 (2020) 39–47
Special Issue on Electrical Machines and Drives

Iranian Journal of Electrical and Electronic Engineering

Journal Homepage: ijeee.iust.ac.ir

Research Paper

# A Novel High-Performance Field-Weakening Control for Axial Flux-Switching Permanent-Magnet Motor

J. Rahmani Fard*(C.A.)

**Abstract:** By combining the field-weakening control principle of a new axial flux-switching permanent-magnet motor (AFFSSPM) with the space vector pulse width modulation (SVPWM) and maximum torque per voltage (MTPV) control principle, a novel field-weakening control strategy for AFFSSPM is proposed in this paper. In the first stage of the field-weakening, the difference between the reference voltage updated by the current regulator and the saturated voltage output with SVPWM is used for field-weakening control, which modifies the direct axis of stator current. This method makes full use of the DC bus voltage, and can naturally smooth transition. In the second stage of the field weakening, the principle of MTPV control is used for field-weakening control, and then, being linearized. Compared with the traditional method, this method solves the problem of depth weakening of AFFSSPM. Between the two stages, the turning speed is used for the switch condition to achieve a smooth transition. The effectiveness and correctness of the proposed field-weakening control method and calculation method were verified with simulation results. Moreover, the dSPACE semi-physical simulation experimental platform for the hardware design and software design is used, and the semi-physical simulation experiment is carried out. The results show the accuracy and effectiveness of the proposed scheme.

**Keywords:** Flux-Switching Permanent-Magnet Motor, Field-Weakening Control, MTPV, Stability.

## 1 Introduction

IN recent years, with the development of power electronics technology and permanent magnet materials, permanent magnet synchronous motors have been widely used in aerospace, rail, water, hydropower, electric vehicles, and other fields, especially under the theme of environmental protection. The application of permanent magnet synchronous motor in pure electric vehicles is very necessary and meaningful [1]. The main features of permanent magnet synchronous motor are high power density, high efficiency, high reliability and weak magnetic control. This is also the result of extensive research on permanent magnet synchronous motors.

Flux-switching permanent magnet motor has got extensive attention owing to high torque density, good fault tolerance capability and other advantages [2-8]. In FSPM motors, magnetic field and armature field are at an angle of 90° to each other and hence, there is no concern about demagnetizing the PMs. Recently, a novel yokeless and segmented armature axial flux-switching sandwiched permanent magnet motor (YASA-AFFSSPM) which has sandwiched-type PMs and an advanced phase group concentrated-coil winding whit unity displacement winding been proposed and investigated in [8].

The improvement of the speed regulation performance of PM synchronous motor is mainly devoted to the motor structure and control method. For the motor structure, researchers have proposed various PM materials and structural improvements to promote the speed control system [9]. For the control method, the control strategy of vector control and field weakening

Iranian Journal of Electrical and Electronic Engineering, 2020.
Paper first received 04 July 2019, revised 05 December 2019, and accepted 13 December 2019.
* The author is with the Department of Power Engineering, Faculty of Electrical Engineering, Pooyesh Institute of Higher Education, Qom, Iran.
E-mail: javad.rahmani.fard@gmail.com.
Corresponding Author: J. Rahmani Fard.

control are proposed to improve the speed control system [10, 11].

The six-step voltage method is proposed in [12]. When the motor is operating in the field weakening area, the phase angle of the motor is controlled. It is used to weaken the magnetic field of the motor, moreover, it is used to adjust the output torque of the motor.

The most widely used method for field-weakening was proposed in [13]. It employs a voltage regulator to improve the id reference so that the current would not lose control. Three regulators work together in the field-weakening region. The control performance is determined by the parameters of the regulators and it is hard to obtain the best parameters for the three regulators simultaneous. Hu Taiyuan proposed a field weakening control method Based on Single Current Regulator and Variable Q-axis Voltage. By making full use of the motor DC voltage, the motor works at the optimal operating points. Thereby improving the efficiency and load capacity of the motor to a certain extent [14].

An adaptive field weakening control method is proposed in [15]. The main idea is to achieve field weakening control by suppressing the current regulator from reaching saturation. The q axis current is controlled by the speed loop of the adaptive field weakening controller for direct model reference, and the d axis current is controlled by the adaptive field weakening controller. When the inverter voltage reaches the maximum value of the DC voltage, the current regulator begins to saturate, thereby controlling the adaptive field weakening controller to generate a certain demagnetizing current to ensure that the d axis current works normally under any conditions.

A field weakening control method is proposed in [16] for transforming the q-axis voltage to single current regulator. By making full use of the motor voltage, the q-axis command value of the motor can track the output torque and speed of the motor in real-time to ensure that the motor works stably as well as possible. So as to improve the efficiency and load capacity of the motor.

The PM synchronous motor speed control is mainly divided into three stages: 1) when the motor speed is below the base speed. Coordinate changes by controlling frequency and voltage to achieve the speed regulation effect. This stage is the constant torque region. 2) When the motor speed reaches above the base speed. Since the motor back electromotive force (back-EMF) is proportional to the speed, the terminal voltage of the motor follows the speed and rises to the maximum voltage value that the inverter can produce, and keeps the rated value unchanged. At this time, if the frequency is adjusted by increasing the frequency, the motor voltage equation will not be established. Therefore, in order to ensure that the voltage equation is constant, the rotor flux of the permanent magnet synchronous motor must be weakened while the frequency is increased. However, the rotor of the PM synchronous motor is a permanent magnet, and the permanent magnetic flux remains unchanged. Therefore, the demagnetizing current can only be applied in the direction of the permanent magnet, and the equivalent permanent magnetic flux is weakened. This stage is the field-weakening zone (I), which is also the constant power region. 3) When the motor speed continues to rise. Since the motor is operated by voltage and current, both voltage and current must not exceed the limits of the voltage limit ellipse and current limit circle. At this time, it is only necessary to ensure that the motor is running at the maximum power state. This stage is field-weakening zone (II), which is also the maximum power output region.

In the constant torque region, the output power is continuously increased. The methods usually used in this area are id=0 control, cosΦ=1 control and maximum torque per current control [17]. The maximum torque per current control can achieve optimal torque control [18]. In the field-weakening zone (I), the output power of the motor is constant, and the output torque is continuously reduced. At this stage, the usual field-weakening strategy is the formula calculation method, the lookup table method, gradient descent method and negative d-axis current compensation method. The formula calculation method relies entirely on the mathematical model of the motor, which has only theoretical significance; the lookup table method needs to rely on a large amount of experimental data, which is difficult to implement; the gradient descent method is quite complicated and have not practical project significance; negative d-axis current compensation method has good parameter robustness and simple calculation, and has been widely used in engineering. This paper adopts the control method of negative d-axis current compensation. In the field-weakening zone (II), the given current value is large, and the motor is in deep demagnetization. If the negative direct current compensation method is used, it is easy to make the actual current unable to track the given current. As a result, the current regulator is rapidly saturated and the current is out of control, so this stage is usually controlled by a method of reducing the q-axis current.

The focus of this paper is to propose a new control method that allows the motor to smoothly transition between the three stages in the case of deep field weakening. The method uses a double closed-loop structure, which makes it easier to achieve no static error adjustment. Using a double regulator structure, the adjustment efficiency is higher than that of the single closed-loop structure, and the torque control capability is stronger. Moreover, the MTPV adjustment is used to improve the depth field-weakening stability.

In order to make the motor smoothly transition between the variable frequency and variable voltage in the field-weakening zone I, a new field-weakening

method, the voltage difference feedback method, is used. This method is the difference between the actual terminal voltage of the motor and the voltage modulated by the voltage space vector. Compared with the traditional voltage feedforward method, voltage feedback method and current difference feedback method, the voltage difference feedback method effectively suppresses the voltage saturation of the current controller, improves the dynamic response capability, and improves the utilization rate of the DC bus voltage. In order to make the motor smoothly transition between the field-weakening zone I and the field-weakening zone II, the maximum torque per voltage control method is adopted in this paper and the curve is linearized. Hence, the current can be made available and control can simplify calculations.

## 2 AFFSSPM Mathematical Model

### 2.1 Configuration of YASA-AFFSSPM Motor

Fig. 1 shows the configuration of the YASA-AFFSSPM with 12 stator slots (S) and 19 rotor poles (P). In this configuration there is not stator yoke, also two rotors are axially unaligned. Moreover, a special concentrated-coil winding, that has displacement winding factor equal to 1, is used [8].

### 2.2 Mathematical Model of AFFSSPM Motor in d-q Coordinate System

The flux linkage equations of the motor can express as

$$\begin{cases} \psi_d = L_d i_d + \psi_f \\ \psi_q = L_q i_q \end{cases} \tag{1}$$

where $\psi_d$ and $\psi_q$ are dq- axes stator flux, $L_d$ and $L_q$ are dq-axes inductances, $\psi_f$ is the rotor permanent magnet flux linkage and $i_d$ and $i_q$ are the dq-axes stator currents. The voltage equations of the motor can express as

$$\begin{cases} u_d = \dfrac{d\psi_d}{dt} - \omega_r \psi_q + R_s i_d \\ u_q = \dfrac{d\psi_q}{dt} + \omega_r \psi_d + R_s i_q \end{cases} \tag{2}$$

where $u_d$ and $u_q$ are the dq-axes stator voltages, $\omega_r$ is the electrical angular velocity and $R_s$ is the armature winding resistance. When motor is statically stable, the derivative of (2) is zero, and from (1) and (2) the steady-state voltage equation of the motor can write as

$$\begin{cases} u_d = -\omega_r L_q i_q + R_s i_d \\ u_q = \omega_r L_d i_d + \omega_r \psi_f + R_s i_q \end{cases} \tag{3}$$

Electromagnetic torque of the motor can express as

$$T_e = \frac{3}{2} N_p [\psi_f i_q - (L_q - L_d) i_d i_q] \tag{4}$$

where $N_p$ is the pole pair of the motor.

### 2.3 Voltage Limit Ellipse and Current Limit Circle

When the motor is running in steady-state, the voltage and current are limited by the maximum voltage and the maximum current, which can express as

$$\begin{cases} u_d^2 + u_q^2 \le U_{smax}^2 \\ i_d^2 + i_q^2 \le I_{smax}^2 \end{cases} \tag{5}$$

When the AFFSSPM motor is running at high speed and stable state, its back-EMF is very large, and the influence of the resistance can be ignored. The resistance term in (3) can be ignored and the Equation can be brought into (5). the voltage limit elliptic equation can express:

$$\begin{cases} (L_d L_d + \omega_f)^2 + (L_q i_d)^2 \le \left(\dfrac{U_{s\max}}{\omega_r}\right)^2 \\ i_d^2 + i_q^2 \le I_{s\max}^2 \end{cases} \tag{6}$$

where $I_{smax}$ is the amplitude of the maximum input current of the motor and $U_{max}$ is the amplitude of the maximum output voltage of the inverter. According to (6), the voltage limit ellipse and current circle at different rotational speeds are plotted in Fig. 2.

## 3 Control Strategy

The block diagram of the whole control system is

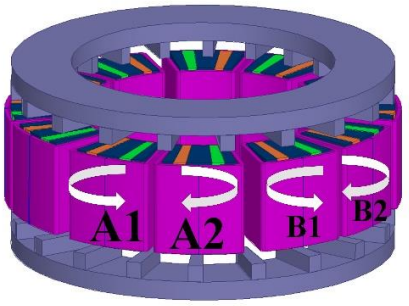


**Fig. 1** Configuration of the YASA-AFFSSPM motor.

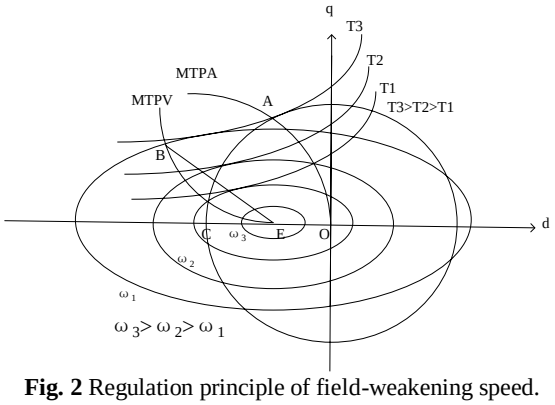


**Fig. 2** Regulation principle of field-weakening speed.

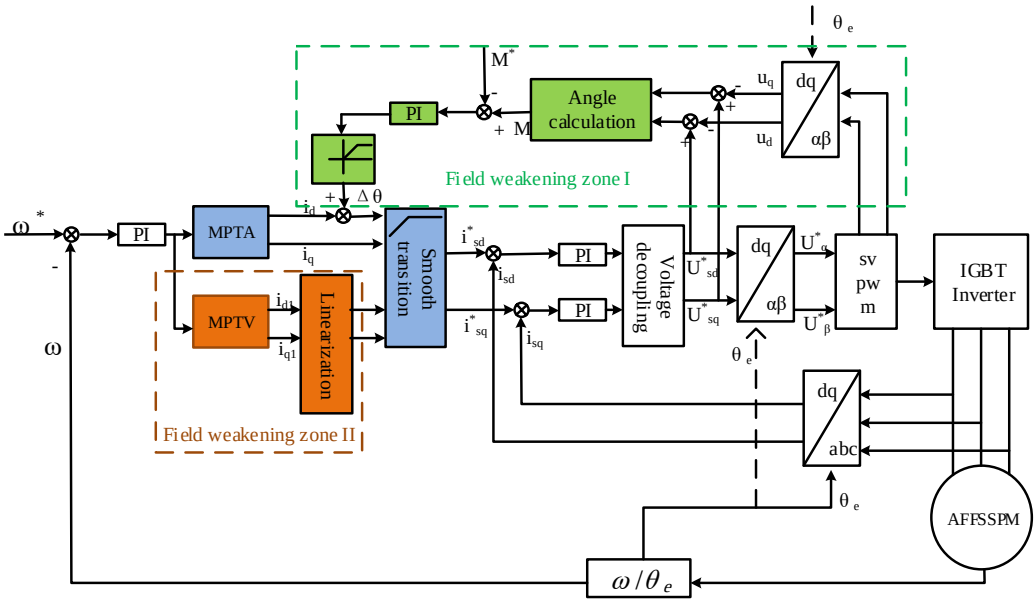


**Fig. 3** Field-weakening control block diagram.

mainly composed of three parts, corresponding to the three stages of the control process as shown in Fig. 3.

### 3.1 Maximum Torque Per Current Control

The maximum torque per current control, also called MTPA control, tries to use the minimum current to generate a given torque, which can be converted into the extreme value problem of the torque equation under the constraint of the current. The current equation is:

$$i_s = \sqrt{i_d^2 + i_q^2} \tag{7}$$

From (4) and (7), a helper function can be introduced according to the Lagrangian extremum principle as

$$H = \lambda\{T_e - \frac{3}{2} N_p [\psi_f + (L_d - L_q) \cdot i_d] \cdot i_q\} + \sqrt{i_d^2 + i_q^2} \tag{8}$$

where λ is the Lagrangian coefficient. Finding the partial derivative of (8) gives the expressions of $i_d$ and $i_q$:

$$\begin{aligned} i_d &= \frac{\psi_f}{2(L_d - L_q)} - \sqrt{\frac{\psi_f^2}{4(L_d - L_q)^2} + i_q^2} \\ i_q &= \sqrt{i_s^2 - i_d^2} \end{aligned} \tag{9}$$

The trajectory of the motor current at this stage is shown in the OA section shown in Fig. 2.

### 3.2 Field-Weakening Zone I

The voltage difference before and after the voltage space vector modulation with SVPWM is used as the feedback amount of $i_d$. After processing, the feedback amount is used as the feedback amount of $i_d$, so that the control curve moves along the AB segment in Fig. 2 to achieve the purpose of weakening. When the motor runs below the base speed, the reference voltage $u_s^*$ is small and is in the regular hexagon. The reference voltage before modulation is equal to the actual output voltage $u_s$ after modulation and the voltage difference between them is zero. As the speed increases, the motor terminal voltage reaches the saturation limit voltage of the inverter output, and the reference voltage will exceed the boundary of the regular hexagon. The actual voltage output after modulation will be less than the reference voltage before modulation, and there is a voltage difference between them. The minimum error overmodulation method is used to adjust the reference voltage, so that it falls within the regular hexagon to track the actual voltage trajectory (Fig. 4). This voltage difference feedback is not dependent on the specific parameters of the motor. It only needs to be automatically weakened according to the speed of the rotation, so that a smooth transition in two stages can be achieved.

In order to fully utilize the DC bus voltage and redistribute the dq-axis current using the difference obtained before and after modulation, it is only necessary to change the current phase angle and set a new phase angle as:

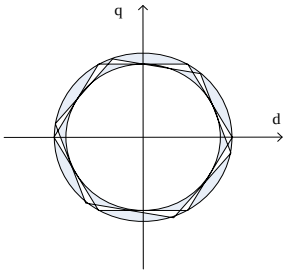


**Fig. 4** SVPWM voltage limit.

$$\theta^* = \theta + \Delta\theta \tag{10}$$

where $\theta$ is the initial phase angle; $\Delta\theta$ is the compensated phase angle; $\theta^*$ is the compensated phase angle. This gives the adjusted current component value:

$$\begin{bmatrix} i_d \\ i_q \end{bmatrix} = i_s \begin{bmatrix} \cos(\theta + \Delta\theta) \\ \sin(\theta + \Delta\theta) \end{bmatrix} \tag{11}$$

The field-weakening zone I of Fig. 3 is an angle calculation module that defines the bus voltage utilization as:

$$M = \frac{\sqrt{u_d^{*2} + u_q^{*2}}}{\sqrt{u_d^2 + u_q^2}} \tag{12}$$

According to the previous description: when the motor speed is less than the base speed, the voltage is equal before and after, that is, $M$=1; when the motor speed is greater than the base speed, the modulated voltage is less than the voltage before modulation, that is, $M$>1. The Given reference quantity $M$* determines the start time of the field-weakening control, the value of $M$* can be slightly larger than 1 or slightly less than 1. The value of $M$* affects the field-weakening starting point. If the value is too small, the motor enters the field-weakening early and will generate excessive oscillation current at the transition point. The value of $M$* can be set according to the specific motor parameters and the actual motor running condition to achieve the optimal field weakening effect.

### 3.3 Field-Weakening Zone II

The traditional voltage feedback field weakening control method can only make the motor run stably in the field-weakening zone I. When the motor runs to point B in Fig. 2, the motor speed is increased, and the motor current curve is still along the current limit circle. In this way, the size of the $i_q$ in the BC segment changes greatly. This large change will cause the vector current and torque to fluctuate greatly. The two current regulators will quickly saturate, causing the system to be extremely unstable. Therefore, when the motor runs to point B, this paper uses the MTPV control method to try to operate the motor along the MTPV curve, and then linearizes the curve. At the same time, a new switch is added. The control point of the switch is the speed of point B. The switch is operated with the B-point motor speed as the turning speed, so that the motor can smoothly transition between the two weak magnetic regions. Like the maximum torque per current, the Lagrange extreme value theorem can be used to solve the curve equation, and the synchronous motor runs on the field-weakening. The voltage constraint satisfied in Zone II is as

$$U_S = \omega_e \sqrt{(L_q i_q)^2 + (L_d i_d + \psi_f)^2} \tag{13}$$

where $\omega_e$ is the electrical angular velocity. Combined with the torque equation (4), a helper function can be introduced according to the Lagrangian extreme value theorem:

$$\begin{aligned} H = {} & \frac{3}{2} N_p [\psi_f + (L_d - L_q) \cdot i_d] \cdot i_q \\ & + \lambda [U_s - \omega_e \sqrt{(L_q i_q)^2 + (L_d i_d + \psi_f)^2}] \end{aligned} \tag{14}$$

Equation (15) was obtained by partial derivatives as

$$\begin{aligned} & 2L_d^2 \cdot i_d^2 + \frac{\psi_f L_d}{L_d - L_q}(4L_d - 3L_q) \cdot i_d \\ & + \frac{\psi_f^2}{L_d - L_q}(2L_d - L_q) - \frac{U_s}{\omega_e} = 0 \end{aligned} \tag{15}$$

The expression of $i_d$ can be solved by (15), and the expression of $i_q$ can be solved by bringing the expression into (13), thereby the MTPV curve equation is obtained. It is known from the appeal process that the calculation process of the current component expression of the MTPV control is very complicated. The curve is now linearized, since point B is the intersection of the MTPV and the current limit circle. The direct current of point B can be calculated as

$$\begin{aligned} i_{db} = {} & -\frac{\psi_f}{L_d} + \frac{-L_q \psi_f}{2L_d(L_d - L_q)} \\ & + \frac{\sqrt{(L_q \psi_f)^2 + 4L_q^2 (L_d - L_q)^2 i_{qb}^2}}{2L_d(L_d - L_q)} \end{aligned} \tag{16}$$

Moreover, $i_{qb}$ can be calculated as

$$i_{dq} = \sqrt{I_{smax}^2 - i_{db}^2} \tag{17}$$

The q-axis current value $i_{bq}$ is obtained, and the coordinates of the intersection point B are obtained. Combining $E(-\psi_f / L_d, 0)$, the slope $k$ of the straight line BE that can be obtained:

$$k = \frac{2L_d(L_d - L_q) \cdot i_{qb}}{\sqrt{L_q \psi_f{}^2 + 4L_q^2 (L_d - L_q)^2 i_{qb}^2} - L_q \psi_f} \tag{18}$$

Then the linear equation is:

$$i_q = k\,(i_d + \frac{\psi_f}{L_d}) \tag{19}$$

After the motor runs to point B, the current curve will be the intersection of the line BE and the voltage limit ellipse at the corresponding speed. This control method makes the motor run on the approximate MTPV curve,

avoiding the possible runaway phenomenon of the current trajectory along the BC curve and combining the transition device a smooth transition between two zones is achieved.

## 4 Simulation Results Analysis

In order to verify the feasibility and correctness of the proposed control method and algorithm, the Matlab/Simulink toolbox is used to establish the system simulation model, and the system is simulated. The simulation parameters of the motor are shown in Table 1.

Fig. 5 is a simulation result of the system when the motor started with rated load and field-weakening expansion speed is above 6000 r/min. It can be seen from the figure that the currents of the d-axis and the q-axis remain basically unchanged before 0.1 seconds, the field-weakening loop has no output, the compensation angle $\Delta\theta$ is zero, $i_d$ is small, and $i_q \approx i_s$, the trajectory is straight line at this stage. As the speed increases, when the speed exceeds 1500 r/min, the motor begins to enter the field weakening region, and the field weakening controller I will generate a negative $\Delta i_d$ feedback to the straight axis. The compensation angle $\Delta\theta$ begins to appear positive and gradually increases. The $i_d$ continuously increases negatively, and the $i_q$ continuously decreases. This stage makes the value of $i_d$ close to the negative nominal current, $i_q$ becomes small. When the speed reaches 6000 r/min, the motor can continue the increasing of the speed through MTPV control. The values of the $i_d$ and the $i_q$ vary little with the increase in the speed. Both $i_d$ and $i_q$ size have a decreasing trend. The current trajectory at this stage is a gentle straight line. Finally, the motor will run stably at around 8000 r/min. As can be seen from the current simulation curve, compared with the traditional permanent magnet synchronous motor field-weakening control, the new control method proposed in this paper has two distinct advantages: the motor can run at higher speeds, and when the motor is running, the current curve fluctuates less and the current is within the controllable range.

### 4.1 Dynamic Performance

Fig. 6 shows the simulated waveforms of the motor speed, dq-axis current components, and torque and a vector diagram of the current trajectory. As can be seen from the Fig.6, the motor torque has two transition zones. The transition from 1500 r/min and 6000 r/min is very smooth. After the motor is stable, the speed and torque curves basically match the given value, and fluctuate is less. It can also be seen from the current trajectory diagram, that the dq-axis current fluctuate is very small. The proposed method achieves a smooth transition from zone 1 to zone 2.

As shown in Fig. 6, when the motor rotates, the torque is always stable during the process of the torque command changes from 18 N.m and 0.5 N.m and then to 2.5 N.m. By tracking the waveforms, it is found that the motor has a good dynamic adjustment performance.

**Table 1** Parameters of the motor.

| Parameter | Value |
|---|---|
| Rated power ($P_N$) [kW] | 1 |
| Rated speed ($N_N$) [r/min] | 1500 |
| Stator resistance ($R_S$) [Ω] | 0.032 |
| d-axis inductance ($L_D$) [MH] | 0.63 |
| q-axis inductance ($L_Q$) [MH] | 0.63 |
| Rotor flux linkage ($\Psi_F$) [Wb] | 0.062 |

## 5 Semi-Physical Simulation Experiment Based on dSPACE

The semi-physical simulation technology is an edge simulation technology between pure digital simulation and physical simulation. It is a partial virtual mathematical simulation model that replaces some physical systems. The semi-physical simulation technology uses a fast real-time simulation algorithm to keep the system time consistent with the actual time, and obtain the external input signal and the simulation process of the external output signal in real time. At present, The semi-physical simulation experiment is carried out on the dSPACE semi-physical simulation

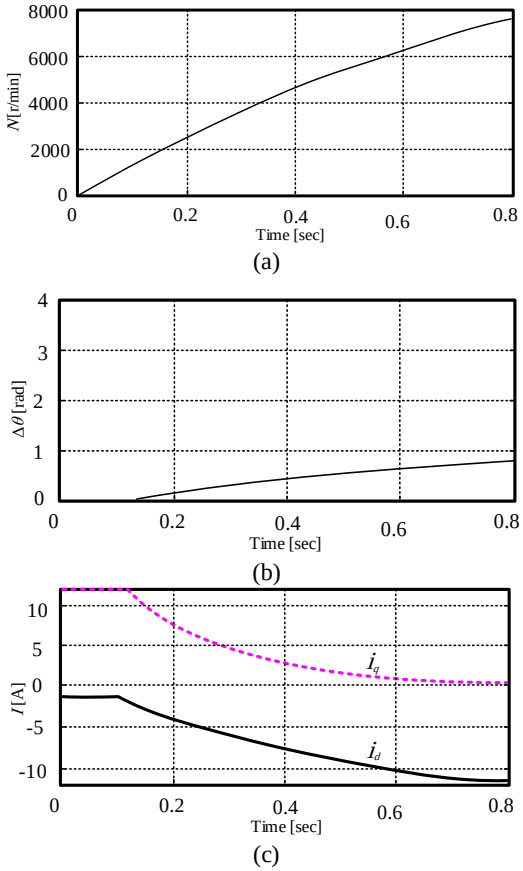


**Fig. 5** Simulation waveform; a) speed, b) compensation angle $\Delta\theta$, and c) $i_d$ and $i_q$.

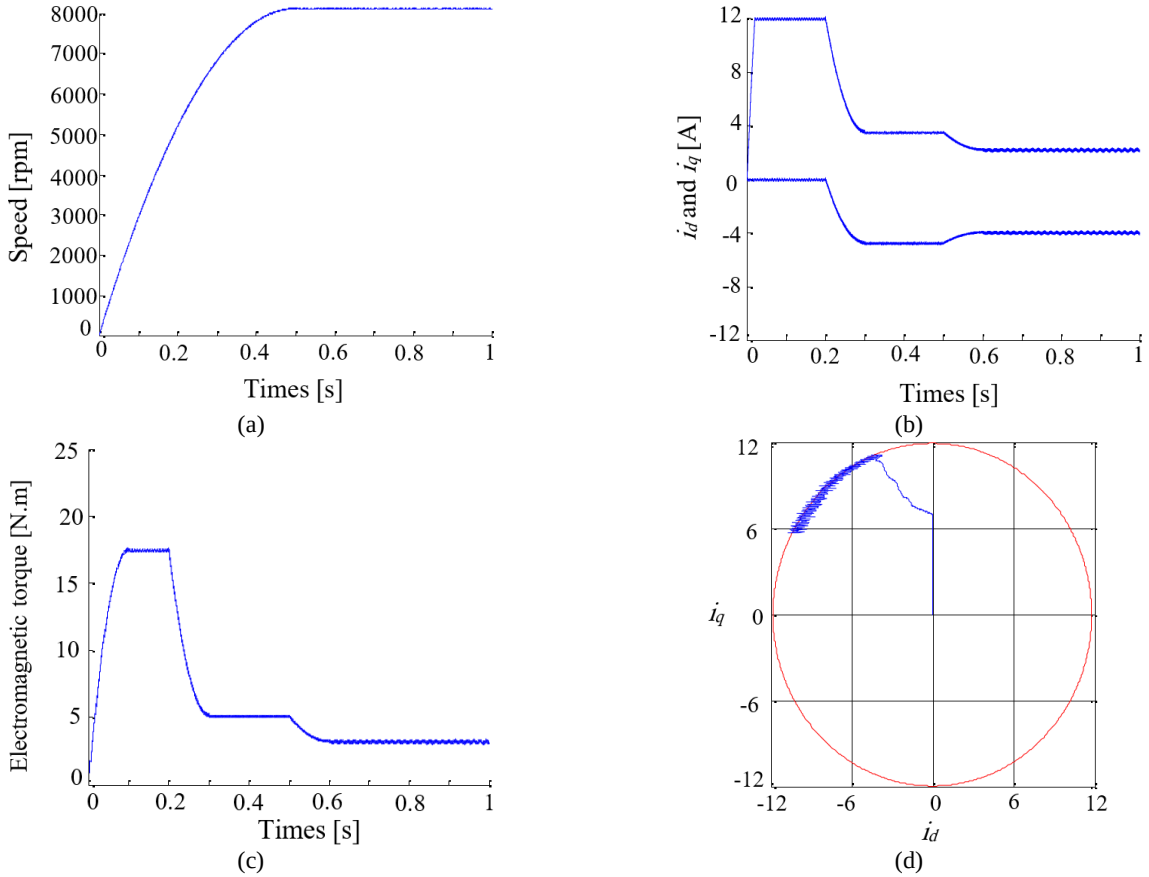


**Fig. 6** a) The speed waveform, b) $i_d$ and $i_q$ current waveforms, c) electromagnetic torque waveform, and d) current vector trajectory.

**Fig. 7** The motor control single board case of in DCU control motor.

**Fig. 8** The Semi physical simulation test platform.

platform. The platform is mainly composed of a simulation computer, dSPACE simulator, I/O interface and drive control unit DCU. The DCU is placed in the traction inverter box and adopts a stacked board structure, including a main control board, a motherboard, an interface board, and adopts a dual OMAP+FPGA+CPLD structure. The trigger pulse is transmitted between the DCU and the inverter module fault signal is fed back to achieve the purpose of controlling the IGBT inverter module. The motor control board in the DCU control chassis is shown in Fig. 7. The semi-physical simulation test platform is shown in Fig. 8.

The steps of the dSPACE semi-physical simulation experiment are as follows:

(1) Using a simulation computer to build a model of a permanent magnet synchronous motor, inverter, and a dynamic in a MATLAB/Simulink environment;

(2) Select the desired I/O port module and set it.

This experiment requires 6 I/O ports to receive the pulse control signal from the DCU, and 6 I/O ports are required to send the motor speed signal to the DCU;

(3) Download the motor and inverter model to dSPACE through the network port. Real-time C code of the target system can be automatically generated by MATLAB/Simulink;

(4) Using the experimental tool software ControlDesk to complete the interaction with the target system;

(5) Monitor and record the experimental waveforms using the host computer monitoring software CSR_Drive.

Fig. 9 shows the dq-axis current, speed at a given speed of 8000 r/min and a given torque of 12 N.m for field weakening control. As can be seen, the system not only has a wide speed range, but also the switching process is stable and the current and torque fluctuations are small, which effectively verifies the correctness of the scheme.

## 6 Conclusion

In this paper, a new method of field weakening control for the axial flux-switching permanent-magnet motor is proposed. This method can make the motor run in the deep weak magnetic field, so that the motor can run at a higher speed. linearized the MTPV curve, and simplified the calculation are the specific feature of this method. At the same time, it is proposed to design a transition device so that the motor can smoothly transition between the weak magnetic regions. The simulation results show that the proposed control strategy is feasible. Moreover, a Semi-physical simulation experiment based on dSPACE is done, which effectively verifies the correctness of the proposed method.

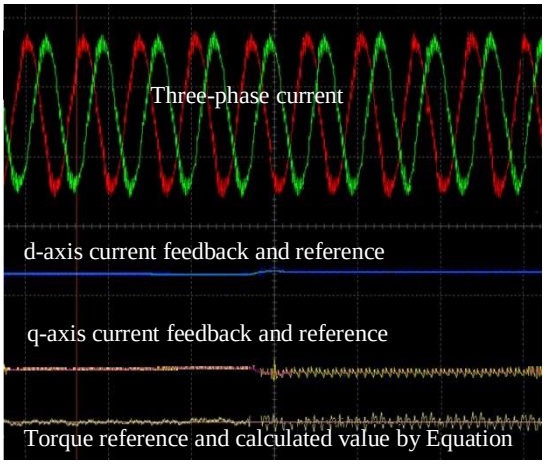


**Fig. 9** Experimental results.

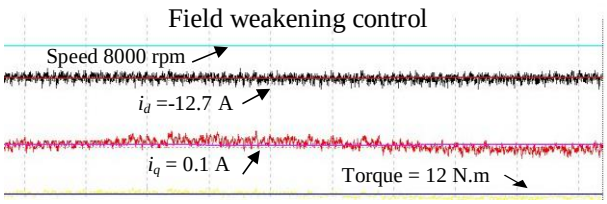


**Fig. 10** Expanded view of Fig. 9.

## References

[1] D. Ying, W. Lixin, and C. Shumei, "Review of the permanent magnet synchronous motor for electrical vehicles," *Micromotor*, Vol. 38, No. 3, pp. 84–86, 2005.

[2] M. Cheng, W. Hua, J. Zhang, and W. Zhao, "Overview of stator-permanent magnet brushless machines," *IEEE Transactions on Industrial Electronics*, Vol. 58, No. 11, pp. 5087–5101, 2011.

[3] L. Hao, M. Lin, W. Li, H. Luo, X. Fu, and P. Jin, "Novel dual-rotor axial field flux-switching permanent magnet machine," *IEEE Transactions on Magnetics*, Vol. 48, No. 11, pp. 4232–4235, 2012.

[4] W. Zhao, T. A. Lipo, and B. I. Kwon, "A novel dual-rotor, axial field, fault-tolerant flux-switching permanent magnet machine with high-torque performance," *IEEE Transactions on Magnetics*, Vol. 51, No. 11, pp. 1–4, 2015.

[5] Y. J. Zhou and Z. Q. Zhu, "Torque density and magnet usage efficiency enhancement of sandwiched switched flux permanent magnet machines using V-shaped magnets," *IEEE Transactions on Magnetics*, Vol. 49, No. 7, pp. 3834–3837, 2013.

[6] J. Rahmani Fard and M. Ardebili, "Sensor-less control of a novel axial flux-switching permanent-magnet motor," *COMPEL-The International Journal for Computation and Mathematics in Electrical and Electronic Engineering*, 2018.

[7] Z. Q. Zhu and J. T. Chen, "Advanced flux-switching permanent magnet brushless machines," *IEEE Transactions on Magnetics*, Vol. 46, No. 6, pp. 1447–1453, 2010.

[8] J. Rahmani Fard and M. Ardebili, "Design and control of a novel yokeless axial flux-switching permanent-magnet motor," *IEEE Transactions on Energy Conversion*, Vol. 34, No. 2, pp. 631–642, 2018.

[9] D. Guan, M. X. Bui, D. Xiao, and M. F. Rahman, "Sensorless control interior permanent-magnet synchronous motor drive over wide speed range operation based on the current derivative method," in *IEEE 20th International Conference on Electrical Machines and Systems (ICEMS)*, pp. 1–6, 2017.

[10] S. Morimoto, Y. Takeda, T. Hirasa, and K. Taniguchi, "Expansion of operating limits for permanent magnet motor by current vector control considering inverter capacity," *IEEE Transactions on Industry Applications*, Vol. 26, No. 5, pp. 866–871, 1990.

[11] Y. Zhang, W. Cao, S. McLoone, and J. Morrow, "Design and flux-weakening control of an interior permanent magnet synchronous motor for electric vehicles," *IEEE Transactions on Applied Superconductivity*, Vol. 26, No. 7, pp. 1–6, 2016.

[12] Y. C. Kwon, S. Kim, and S. K. Sul, "Six-step operation of PMSM with instantaneous current control," *IEEE Transactions on Industry Applications*, Vol. 50, No. 4, pp. 2614–2625, 2014.

[13] J. M. Kim and S. K. Sul, "Speed control of interior permanent magnet synchronous motor drive for the flux weakening operation," *IEEE Transactions on Industry Applications*, Vol. 33, No. 1, pp. 43–48, 1997.

[14] T. Hu, F. Lin, K. Lin, X. Feng, and Z. Yang, "Flux-weakening control of PMSM based on single current regulator and variable q-axis voltage," in *IEEE 15th Internation Conference on Electrical Machines and Systems (ICEMS2012)*, Sapporo, Japan, pp. 20–25, 2012.

[15] J. L. Shi, T. H. Liu, and S. H. Yang, "Nonlinear-controller design for an interior-permanent-magnet synchronous motor including field-weakening operation," *IET Electric Power Applications*, Vol. 1, No. 1, pp. 119–126, 2007.

[16] K. Chen, Y. Sun, and B. Liu, "Interior permanent magnet synchronous motor linear field-weakening control," *IEEE Transactions on Energy Conversion*, Vol. 31, No. 1, pp. 159–164, 2015.

[17] S. Morimoto, M. Sanada, and Y. Takeda, "Wide-speed operation of interior permanent magnet synchronous motors with high-performance current regulator," *IEEE Transactions on Industry Applications*, Vol. 30, No. 4, pp. 920–926, 1994.

[18] M. Lu, Y. Zhang, Y. Wu, X. Cai, and H. Li, "Optimization of MTPA algorithm of permanent magnet synchronous motor for electric tractor," in *IEEE 21st International Conference on Electrical Machines and Systems (ICEMS)*, pp. 371–375, 2018.

**J. Rahmani Fard** received the M.Sc. degree and Ph.D. degree from the K. N. Toosi University of Technology, Tehran, Iran, in 2012 and 2018, respectively, both in Electrical Engineering. He is currently an Assistant Professor, Electrical Engineering Department, Pooyesh Institute of Higher Education, Qom, Iran. His research interests include electrical machines and drives, magnetic materials, design and modeling of permanent magnet machines, and wind generators.